NASA/TM–20250008367

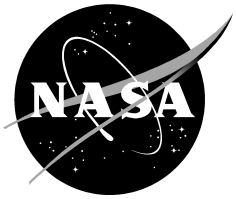

The Mars Aerial Navigation Terrain & Atmosphere (MANTA) Explorer

* *All authors contributed equally to this memo. The names are listed alphabetically by last name.*

Kundana Addala
Liberal Arts and Science Academy, Austin, Texas

Daniel Guo
The Bishop's School, La Jolla, California

Aarav Mann
The Harker School, San Jose, California

Samadrita Mukherjee
Prosper High School, Celina, Texas

Lauren Rodriguez
La Salle College Preparatory, Pasadena, California

Avaneesh Savarala
Novi High School, Novi, Michigan

Tobias Stone
Manheim Township High School, Lancaster, Pennsylvania

August 2025

NASA STI Program Report Series

The NASA STI Program collects, organizes, provides for archiving, and disseminates NASA's STI. The NASA STI program provides access to the NTRS Registered and its public interface, the NASA Technical Reports Server, thus providing one of the largest collections of aeronautical and space science STI in the world. Results are published in both non-NASA channels and by NASA in the NASA STI Report Series, which includes the following report types:

- TECHNICAL PUBLICATION. Reports of completed research or a major significant phase of research that present the results of NASA Programs and include extensive data or theoretical analysis. Includes compilations of significant scientific and technical data and information deemed to be of continuing reference value. NASA counter-part of peer-reviewed formal professional papers but has less stringent limitations on manuscript length and extent of graphic presentations.

- TECHNICAL MEMORANDUM. Scientific and technical findings that are preliminary or of specialized interest, e.g., quick release reports, working papers, and bibliographies that contain minimal annotation. Does not contain extensive analysis.

- CONTRACTOR REPORT. Scientific and technical findings by NASA-sponsored contractors and grantees.

- CONFERENCE PUBLICATION. Collected papers from scientific and technical conferences, symposia, seminars, or other meetings sponsored or co-sponsored by NASA.

- SPECIAL PUBLICATION. Scientific, technical, or historical information from NASA programs, projects, and missions, often concerned with subjects having substantial public interest.

- TECHNICAL TRANSLATION. English-language translations of foreign scientific and technical material pertinent to NASA's mission.

Specialized services also include organizing and publishing research results, distributing specialized research announcements and feeds, providing information desk and personal search support, and enabling data exchange services.

For more information about the NASA STI program, see the following:

- Access the NASA STI program home page at http://www.sti.nasa.gov

- Help desk contact information:

https://www.sti.nasa.gov/sti-contact-form/ and select the "General" help request type.

NASA/TM–20250008367

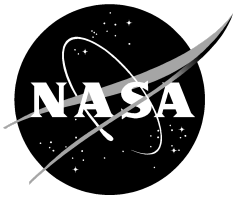

The Mars Aerial Navigation Terrain & Atmosphere (MANTA) Explorer

** All authors contributed equally to this memo. The names are listed alphabetically by last name.*

Kundana Addala
Liberal Arts and Science Academy, Austin, Texas

Daniel Guo
The Bishop's School, La Jolla, California

Aarav Mann
The Harker School, San Jose, California

Samadrita Mukherjee
Prosper High School, Celina, Texas

Lauren Rodriguez
La Salle College Preparatory, Pasadena, California

Avaneesh Savarala
Novi High School, Novi, Michigan

Tobias Stone
Manheim Township High School, Lancaster, Pennsylvania

National Aeronautics and Space Administration
Ames Research Center, Mountain View, CA

August 2025

Acknowledgments

We want to start off by thanking our mentors, Alexey Munishkin and Raj Pai, for guiding us throughout the entire process of assembling this report and concept. They provided invaluable insights and there was no way we could have finished this project without their help. We would also like to thank Shannon Zelinski for running the Aviation Concept Design Program. Finally, we would like to thank everyone at the Ames Research Center for welcoming us during our in-person visit and for making our experiences in this program an amazing one.

Table of Contents

Abstract....7
Introduction....8
Background....9
    History of Mars Exploration....9
    Challenges During Previous Missions....10
Concept of Operations....11
    Assumptions and Constraints....11
    Impact....12
    Scenarios of Use....13
Methods....14
Results & Analysis....14
    Flight Simulations....14
    Rotor Configuration Models....16
    Path Planning Models....19
Design....22
    Aeronautics....22
    Power Supply & Consumption....24
    Materials....29
    Scientific & Navigation Instruments....30
    Software....34
Mission Goals....41
Conclusion & Recommendations....44
References....46

Abstract

Over the last half century, Martian exploration has continuously uncovered answers to some of our longest held questions about both our solar system and the Red Planet. With the completion of the Ingenuity mission in January 2024, a new era of planetary science has begun, one centered around aerial exploration. Rovers and orbiters have dominated the last two decades of Mars missions and have yielded unprecedented findings, but they have created a gap between the detailed-oriented nature of terrestrial exploration and the broader, planetary-wide research being conducted from orbit. For these reasons, the Mars Aerial Navigation Terrain & Atmosphere (MANTA) Explorer is proposed as a mission concept to explore large portions of the planet from the atmosphere while collecting invaluable, detailed geological, atmospheric, and technical information about Mars. Through simulations and 3D modeling, the feasibility of the aircraft in this environment was tested while considering the scientific objectives of the mission. From these results, the MANTA Explorer was developed to be a versatile, fixed-wing aircraft with vertical takeoff and landing (VTOL) capabilities that would allow it to travel and land in diverse and hard to reach locations. Alongside these technical aspects, advanced artificial intelligence/machine learning (AI/ML) applications for flight planning, obstacle avoidance, and VTOL will be at the heart of this mission. Scientific and navigational sensors will be employed to further investigate the unique geology of the planet while mapping its terrain in extreme detail and probing for potential locations of subterranean or frozen water. MANTA ultimately aims to deepen our understanding of the Red Planet while demonstrating the technical applications of fixed-wing flight and AI/ML in extraterrestrial exploration.

Introduction

Mars has undoubtedly become the next frontier in space exploration. As humanity expands its understanding of the Red Planet, we continue to realize its true scientific wealth. For decades, both the National Aeronautics and Space Administration (NASA) and non-NASA missions have made monumental discoveries, answering many questions while simultaneously prompting us to ask even more. This paper will aim to explore the wicked problem “How can Mars be effectively and efficiently explored autonomously?” Like all wicked problems, there is no single answer and it often requires multiple approaches working in tandem. While Mars has been explored autonomously for over 60 years, only in the last few has it been explored from the air. To further address the wicked problem, this paper builds upon the work of the Ingenuity helicopter by proposing a conceptual aircraft to explore Mars from above [1].

The Mars Aerial Navigation Terrain & Atmosphere (MANTA) Explorer is a mission concept for an unmanned aerial vehicle (UAV) designed to fly and operate in the Martian atmosphere. The MANTA Explorer gets its name from the manta ray, a large aquatic animal that gracefully glides through the ocean with its large wingspan, flat body, and intelligent mind [2]. One of the major limitations of using rovers as the primary means of Mars exploration is that throughout a rover’s lifetime, it will only travel a few dozen kilometers. This UAV will remedy this issue and potentially travel tens of thousands of kilometers while on Mars, collecting terrain and atmospheric data about the planet at an unprecedented scale with a level of accuracy and detail not possible of Mars orbiters.

From a technical standpoint, the MANTA Explorer is designed to overcome one of the major challenges of flight on Mars: generating sufficient lift in the thin atmosphere to allow for sustained flight. Using vertical takeoff and landing (VTOL) and an airfoil uniquely designed for the low Reynolds number environment, MANTA aims to extend the research capabilities of Martian missions while acting as a technical demonstration for fixed-wing flight on Mars. While key design elements– power supply, artificial intelligence/machine learning (AI/ML) applications, scientific sensors, material composition, and navigational techniques– will be analyzed and discussed later, it is clear that the use of UAVs represents NASA’s next major step in extraterrestrial

exploration– a step that will redefine our understanding of Mars, the solar system, and even our own planet.

Background

History of Mars Exploration

When the first man-made objects reached space in the 1940s, humans could only dream of reaching Mars. Located 140 million miles from Earth, the Red Planet was a foreign, hostile place, the exploration of which required technologies that did not yet exist. Technological advancements of the 1950s and the start of the space race made Mars exploration possible. The USSR became the first to attempt reaching Mars, with all their missions in the early 1960s being unsuccessful. NASA's Mariner 4 became the first successful mission to Mars in 1964, returning the first close up images of the planet. The missions of the following decade were primarily flybys and orbiters, mapping the surface and studying the atmosphere. In this time, there were several attempts at landers, with the USSR's Mars 3 Lander completing the first soft landing in 1971 and NASA's Viking missions becoming the first successful landers in 1975. After a gap in missions from 1976 to 1987 and the collapse of the Soviet Union, the next successful Mars mission, NASA's Mars Global Surveyor (1996), found liquid water flowing in short bursts on hillsides. That same year, Sojourner became the first Mars rover, kicking off three decades of NASA and United States (U.S.) dominance in Mars exploration. The late 1990s into the 2000s saw a few Japanese and European Mars exploration attempts. In the 2000s, NASA launched the Spirit and Opportunity rovers, along with several orbiters and landers. All of these missions remained active much longer than expected, collecting valuable data about soil, rock, and atmosphere compositions. Since 2011, Mars exploration has become an international goal, as India's Mangalyaan (2013), the United Arab Emirates's (UAE) Hope (2020), and the European Space Agency's (ESA) ExoMars (2016) have all been very successful. As of 2025, China is the only nation besides the U.S. to have successfully landed a rover on Mars, as they did so with the Zhurong rover during their 2020 Tianwen 1 mission. NASA's Curiosity (2012)

and Perseverance (2020) rovers continue to collect data on the surface [3]. When Perseverance was launched in 2020, it was accompanied by the Ingenuity helicopter, the only extraterrestrial aircraft to perform powered and controlled flight. Ingenuity, a small, two kilogram autonomous aircraft, completed seventy-two flights before a temporary loss of communications with Perseverance caused it to crash in January 2024, damaging a propeller blade [1]. NASA will build on this mission's achievements with Dragonfly (2028), a mission that will fly on Titan. NASA, Japan Aerospace Exploration Agency (JAXA), and ESA all have Mars missions planned through 2028 and beyond [3]. One of these proposed missions, CoFlow Jet and NASA's Mars Aerial and Ground Global Intelligent Explorer (MAGGIE), is a forward flight, solar-powered, and VTOL aircraft designed to fly on Mars. MAGGIE has received funding from NASA Innovative Advanced Concepts (NIAC) 2024 Phase I and the concept will continue to be developed by the private company [4]. Innovative missions and mission concepts, like Ingenuity and MAGGIE, inspired the development of the MANTA Explorer with the goal of furthering Martian exploration.

Challenges During Previous Missions

Sending a spacecraft to Mars involves overcoming a variety of challenges. Twenty-six of fifty-one Mars missions have failed outright or failed to meet their planned mission lengths. By examining some of these issues, we hope to develop solutions to them that would prevent MANTA, and future missions, from facing similar fates. Challenges range from possible technical failures to environmental conditions. Frequent technical failures include communication, mechanical, and computer issues. Mechanical issues ranging from booster and shielding separation malfunctions to faulty parts are the primary culprits behind mission failures. Loss of communications has been attributed to mechanical failures as well as computational errors [2]. For a fixed-wing aircraft, however, the biggest challenges are the environmental conditions of Mars. Mars has a thin atmosphere composed of 96% carbon dioxide, 1.9% argon, 1.9% nitrogen, and various trace gases [5]. This atmosphere poses a risk not only for entry, as less drag is created, but also for flight. Mars' atmosphere also allows solar heat to escape, causing drastic changes in temperature with little altitude gain. These temperatures range from -153℃ to 20℃ [6]. The lack of a magnetic field allows Galactic Cosmic Rays

(GCRs) and Solar Energetic Particles (SEPs) to reach the surface. GCRs in particular are a major concern, as they are the primary background radiation and have a high ability to penetrate the internals of an aircraft. However, the largest challenge is airborne dust particles. These fine, iron-rich particles settle on surfaces, potentially blocking equipment from functioning. In addition, unpredictable wind events, ranging from dust devils that last only a few minutes to global dust storms lasting months, can have winds up to 96.6 kph [7].

Concept of Operations

The concept of operations will serve to address the specifications and scope of the MANTA mission concept and provide details to aid in bridging the gap between technical requirements and the goals of this project.

Assumptions and Constraints

This section outlines the different assumptions and constraints that were used when designing the MANTA Explorer. This section's goal is to establish a communal understanding of what this concept is and is not trying to accomplish. The following assumptions include engineering challenges that may arise during construction and transportation that this report will not address, specific scenarios that may occur on Mars that are too extreme and were not taken into account, and administrative issues that could impede this concept's further development. This report will assume that the UAV can be physically constructed without running into material constraints originating from quantity available or price. This paper will mention but not consider the cost of various included components. In regards to transportation of the vehicle to Mars, it will be assumed that it is possible to safely land the object on the surface, most likely using the Sky Crane system, regardless of weight, size, or rocket availability [8]. This is being stated in order to not limit the design of the UAV in wingspan. Finally, it is assumed that, while MANTA is on Mars, no catastrophic events will occur that could jeopardize the

mission. These events include, but are not limited to, marsquakes, powerful solar flares, landslides, and long-duration dust storms.

When designing this concept, multiple constraints were put in place to challenge the current limitation of powered flight on extraterrestrial bodies and specifically Mars. The design of MANTA will be constrained by the fact that the vehicle must be able to perform forward flight for extended periods of time and for long durations. The vehicle must be able to handle flying in the Martian environment with pressures around 0.017 $\frac{kg}{m^3}$ (~675 Pa) and varying temperatures. With regards to flight, the UAV must be able to land and take off on varying rocky terrains [9]. In addition, this concept must be able to remain operable for at least 6 years on Mars. This minimum lifespan of 6 years means that MANTA must survive all the Martian seasons along with any small to large dust storms that impact it during its mission. It should be noted that the stated mission length is simply a minimum and the aircraft, like many other NASA missions, will aim to stay functional for many years past the designated mission timeframe. Finally when designing this concept, it will be the goal to use only existing technologies or innovations that will become available in the near future.

Impact

A variety of useful results have the ability of coming out of the MANTA mission/concept, beyond simply gaining more knowledge on Mars. One of the probable impacts is further advancements in aircraft design and AI/ML use in space exploration, especially since contact or communication between Mars and Earth is prone to delays of up to twenty minutes [10]. MANTA will build upon Ingenuity's path planning algorithms in order to avoid a similar crash to what was detailed in the background section [1]. This project will therefore give insight on flight path planning, safe landing sites, and methods for exploring generally inaccessible areas. Technological innovations will also flourish from data collecting systems, informing future scientific design for aerial endeavors, and future missions to Mars or any extraterrestrial body could use this concept as a guide to navigate their projects and manage their resources. In pursuit of this informative objective of the MANTA project, a great deal of design aspects were determined by referencing the innovative Ingenuity helicopter and MAGGIE plane [1, 4]. Because of

this, and other similarities, we seek to distinguish this explorer from, specifically, the MAGGIE concept and explain how our report differs from this work of CoFlow Jets. MAGGIE is a promising but relatively limited concept that exclusively looked into the use of deflective slipstream technologies for VTOL and other aeronautical functions on Mars. As will be seen throughout this paper, the MANTA project is instead examining all aspects of an aerial mission to Mars (i.e. software, sensors, communication, material, aeronautics, energy consumption, ect.) instead of limiting ourselves to just the aerospace parts. In addition, this concept will use tilting rotors and consider nuclear battery power options instead of the deflective slipstream techniques and solely solar powered design of MAGGIE [4]. Above all, however, this mission concept will impact planetary exploration by developing conceptual systems/ideas to help determine possible past and future habitability on Mars through analysis of its atmospheric and geological conditions.

Scenarios of Use

The MANTA Explorer will be designed to fly and operate in the Martian atmosphere and will be optimized for long duration, fixed-wing flight at varying altitudes and across diverse terrain. This mission was designed to explore and answer current scientific and technical knowledge gaps and, for those reasons, would be most reasonably used in the near future of planetary exploration. This concept will spend a majority of its life stationary on the ground, but when it does fly, it will take off using VTOL mechanisms and then transition to forward flight. The vehicle will stay airborne for an extended duration and complete set flight patterns and pre-programmed routes with its flight planning software adhering to these instructions while also making autonomous decisions. As of locations of use across Mars, MANTA will be able to travel a significant amount of distance throughout its lifetime and could easily be used in most regions of the planet. However, the vehicle has not been designed to operate in the extreme high points and low points of the Martian terrain (i.e. Olympus Mons or Valles Marineris). In addition, flight in Mars' polar regions has not been considered and would be especially difficult with a solar powered design [6].

Methods

This report draws upon diverse sources of quantitative and qualitative data for many of its sections and particularly in the following one where aspects of the design of MANTA are tested and modeled in realistic simulations. Once these data points are collected and results are determined and analyzed, the chosen specifications are listed and described in the design section. The following is a list of the applications used to model aspects of the mission and find the aforementioned results. To complete Computational Fluid Dynamics (CFD) flight simulations and determine the ideal airfoil and Reynolds number, the OpenFOAM application was used [11]. To complete the software-related tests and simulations, a number of toolkits and models were used including matplotlib.pyplot, Axes3D, and Mars_HRSC_MOLA_BlendDEM_Global_200mp_v2 [12, 13, 14]. All of these software applications run on Google Colab [15].

When conducting these tests and making this report, a number of errors arose from a variety of sources and issues out of the scope of this paper. They primarily revolved around the limited timespan given to write and publish this report. Other than from time constraints, possible errors could have come from modeling softwares, human mistakes made when performing calculations or designing this concept, and the limited size of the team developing the MANTA Explorer.

Results & Analysis

Flight Simulations

In order to fly using fixed-wings on Mars, MANTA's airfoil must be designed with low Reynolds numbers (Re) ($10^4 - 10^5$) in mind since the low wind speed and low density of the atmosphere creates highly laminar flow which changes the flight mechanics when compared to that of Earth. To model this, CFD simulations were used to compare the performance of airfoils in low Re regimes. Previous research has indicated that highly undercambered airfoils resembling curved plates have higher

performance at low Re [16]. Therefore, simulations were conducted on a NACA 5502 airfoil that meets these specifications [17]. Using OPENFOAM's standard incompressible steady state solver with Reynolds Averaged Navier-Stokes turbulence modeling, lift and drag coefficients were calculated [11].

Figure 1 shows the flow around the airfoil at 5 degrees angle of attack and Re = 10^4. There is both a laminar separation bubble at the front of the airfoil, as well as trailing edge separation. The magnitude of the laminar separation bubble increases as the angle of attack increases, but at this Re, it reattaches to the airfoil. Simulations show that the determining factor for the lift drag ratio is the trailing edge separation. As the flow separates from the airfoil, drag significantly increases and airfoil performance goes downhill. The amount of trailing edge separation depends on both the turbulent intensity as well as the turbulent length scale. Standard numbers were used for this simulation, but further research is needed to properly model the boundary layer [11].

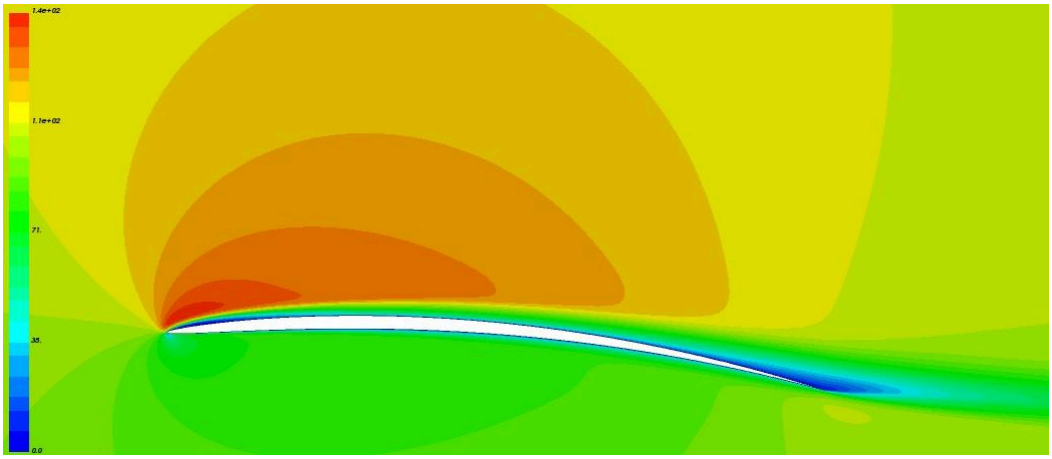

Fig. 1. NACC 5502 airfoil at 5 degree angle of attack with Re = 10^4. Laminar separation bubbles are shown in the front (red-orange region) and back (blue region) [11].

In conclusion, this airfoil would perform well in the Martian environment due to its flat, curved design and small laminar separation bubbles. As was mentioned, additional aspects will require further research to determine precise specifications of the wing design beyond the airfoil shape.

Rotor Configuration Models

The MANTA Explorer is going to be propelled by a series of rotors that can pivot between a position parallel to the ground, needed for VTOL, and a position perpendicular to the ground, needed for forward flight. These calculations and models will assume that each of the propellers have 2 blades and are similar to the Ingenuity rotors in airfoil and other design aspects. To determine the ideal number of rotors and their associate diameter, figure 2 and 3 were created. In both graphs, the blue slope shows this relation by using the following equation.

$$D = \sqrt{\frac{14.8 \cdot m}{\pi \cdot v^2 \cdot N_{rotor} \cdot \rho \cdot CT}}$$

The diameter (D) is in meters, the rotor number is N_{rotor}, constant of thrust (CT) is set at 0.02, the rotor speed (v) is 320 $\frac{m}{s}$ (based off of Ingenuity helicopter), the air density (ρ) is 0.017 $\frac{kg}{m^3}$, and the mass of MANTA (m) is set at 300 kg [1, 9]. Since this equation is giving the needed rotor diameter to produce enough thrust to equal the weight of the UAV, any configuration selected would need to be above the blue slope on the graph. When looking at figure 2, the point should ideally not be too far above the line in order to not over design the rotor systems. In addition, the red slope in this figure is the weight of the rotors assuming that the mass scales linearly from that of the Ingenuity propellers.

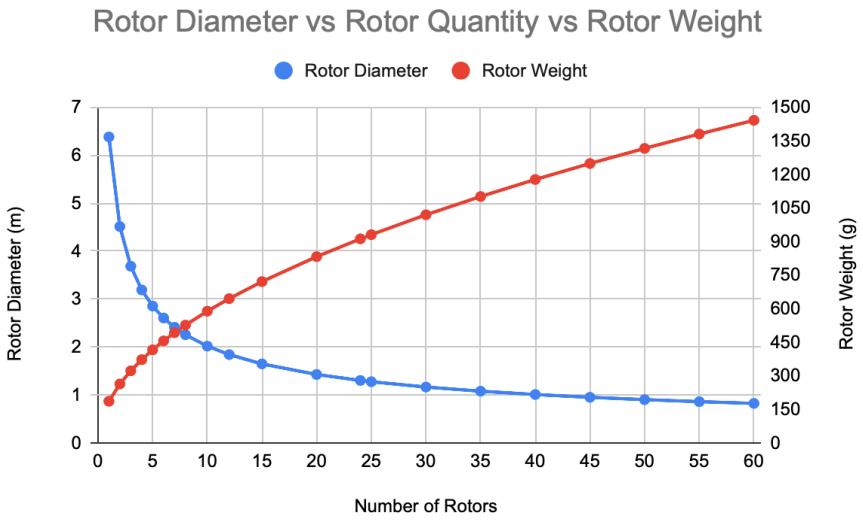

Fig. 2. Relationship between minimum rotor diameter (m) for number of rotors with the weight of each configuration (g) being shown.

In figure 2, the intersection of the two slopes is not meaningful and this graph is only useful in determining the weight of a configuration and relating rotor number to diameter. However, this is not the case in figure 3 that shows rotor efficiency with a yellow slope in addition to the blue slope that compares rotor number to diameter. This efficiency of the rotor systems was found by calculating the maximum thrust (N) over the energy consumed (W). The intersection of these two slopes is meaningful in this figure because it represents the most efficient design that is still able to generate enough thrust to lift the aircraft.

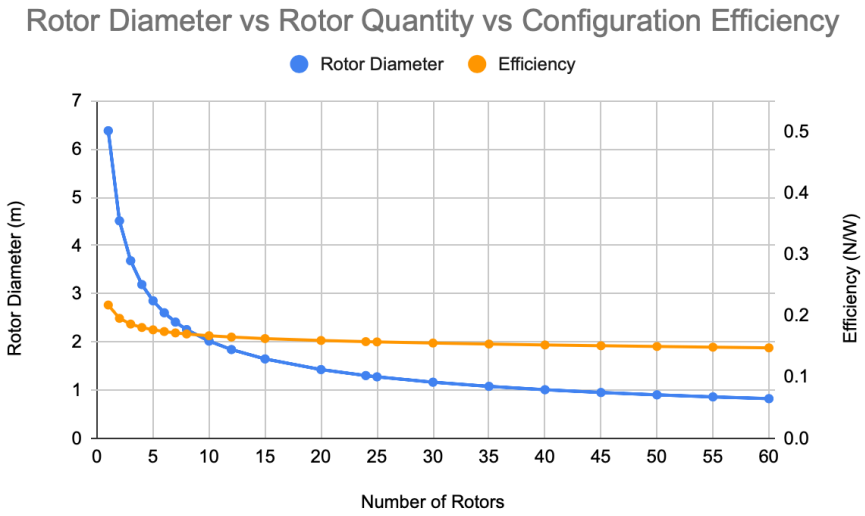

Fig. 3. Relates rotor diameter to rotor number and shows the configurations' efficiencies in $\frac{N}{W}$ with a high number yielding better results in flight.

The final graph, figure 4, shows the tip velocity of the rotor blades at different diameters. The purple slope shows the minimum speed (in rpm) that the rotor blades of each diameter can travel at in order to create enough force for flight. The green slope shows the maximum velocity of the rotor tips (in rpm) before they break the Martian sound barrier at 869 kph [9]. As the rotor diameters increase, slower speeds are needed to break the sound barrier while, at the same time, slower speeds are needed to generate sufficient lift. These slopes decrease at different rates and at some point they will get too close for that rotor configuration to be viable. Any rpm in between the green and purple slopes is a plausible tip speed for the rotor configurations of that diameter and number.

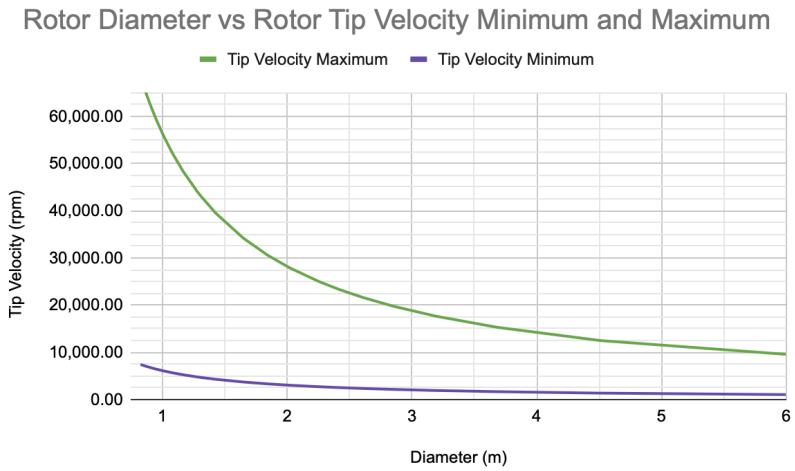

Fig, 4. The minimum and maximum tip velocity, in rpm, of each diameter of rotor blades as part of its associated rotor configuration can be seen with the blue slope in figures 2 and 3.

Path Planning Models

In order to develop flight planning software for MANTA that adapts to obstacles on its route, a simple environment was created to demonstrate the Q-learning approach for reinforcement learning [18]. This environment is visualized by us in figure 5. The 3D map represents space in Mars with altitude (z), latitude (x), and longitude (y). Obstacles represent hazards like high ridges, while the no-fly zones are dangerous because of possible known atmospheric conditions on Mars such as dust storms. The agent (UAV) learns to take the best path based from “Start to Goal “ using Q-learning. The reward system was reaching the goal (+500 points), going through obstacles (-100 points), going through no-fly zones (-50 points). This simulation, seen in figures 5 and 6, proved the feasibility of a basic Q-learning approach [12, 13, 14].

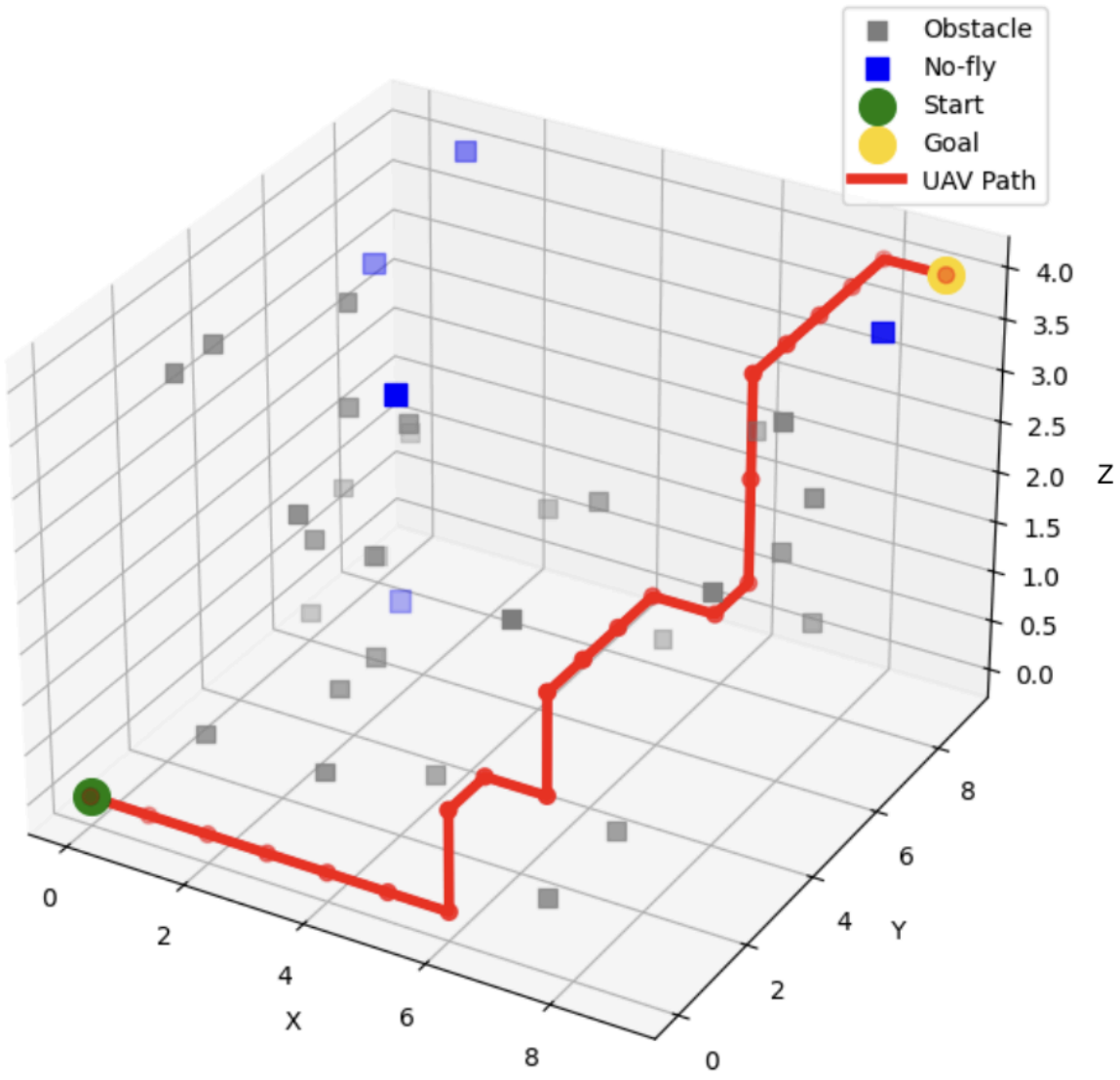

Fig. 5. Learned 3D path (mars-like grid) [12, 13, 14, 15].

```
Q-table values for all z at x=1, y=1:
Q[1, 1, 0, :] = [58.89343751 -6.68730065 39.07019657 -6.64499709 -6.26783869 34.53540232]
Q[1, 1, 1, :] = [66.54775569 -6.60235428 -6.1120506  -6.34110785 -6.09538658 34.52874785]
Q[1, 1, 2, :] = [-5.72992326 -6.02306615 -5.80307517 -5.72373935 -5.76467677 -5.95801148]
Q[1, 1, 3, :] = [-5.69955457 -5.83884619 -5.62257547 -5.94381315 -5.6739051  -5.57967348]
Q[1, 1, 4, :] = [0. 0. 0. 0. 0. 0.]

Q-table values for all actions at (x=0, y=0) over different altitudes:
z=0: [45.80368446 40.22330425 35.20077305 40.22331601 35.19777264 40.22331599]
z=1: [34.34969569 -6.74140868 -6.63175591 -6.900524   -6.65749225 40.22303937]
z=2: [-6.30686009 -6.36433359 -6.30116073 -6.41756956 -6.32956524 -6.84273554]
z=3: [-6.01500748 -6.0443219  -6.0648233  -6.14679993 -6.06918418 -6.42302896]
z=4: [-5.83064636 -5.74829298 -5.89902879 -5.79191569 -5.775448   -5.82291054]
```

Fig. 6. Learned Q-values for initial approach. Approach can be visualized in figure 5 [12, 13, 14, 15].

Next, a Deep Q-Network (DQN) model was trained on 5,000 episodes which can be seen in figure 7. This created a more complex environment for the agent to train and to attempt to optimize certain values. The agent used the epsilon greedy policy [12, 13, 14].

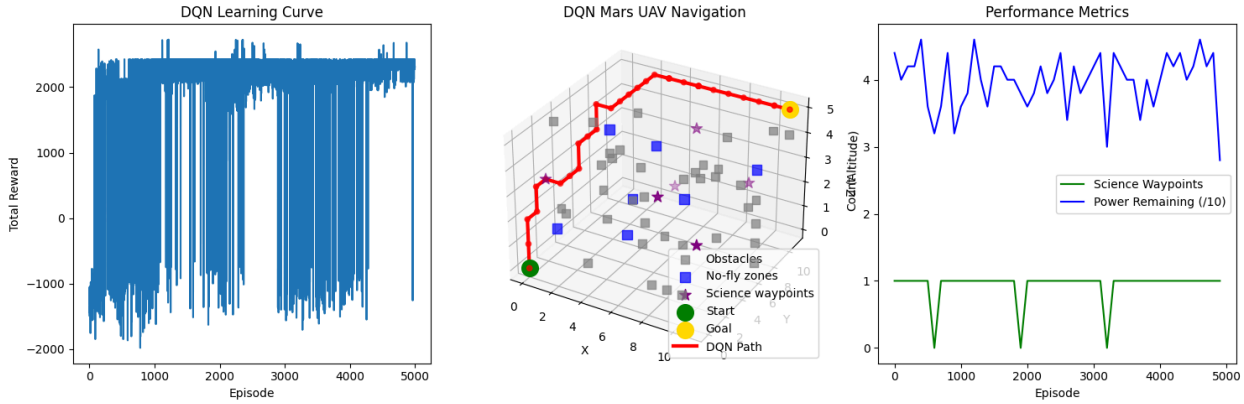

Fig. 7. The learning curve, example path plan, and performance metrics (science waypoints and power remaining) for the episodes [12, 13, 14, 15].

State-Action-Reward-State-Action (SARSA) was also trained in a similar matter but on 100,000 episodes compared to the 5,000 the DQN model trained on. This yielded the results shown below with total reward, average science points, energy conserved, and the best path visible in figure 8 [12, 13, 14].

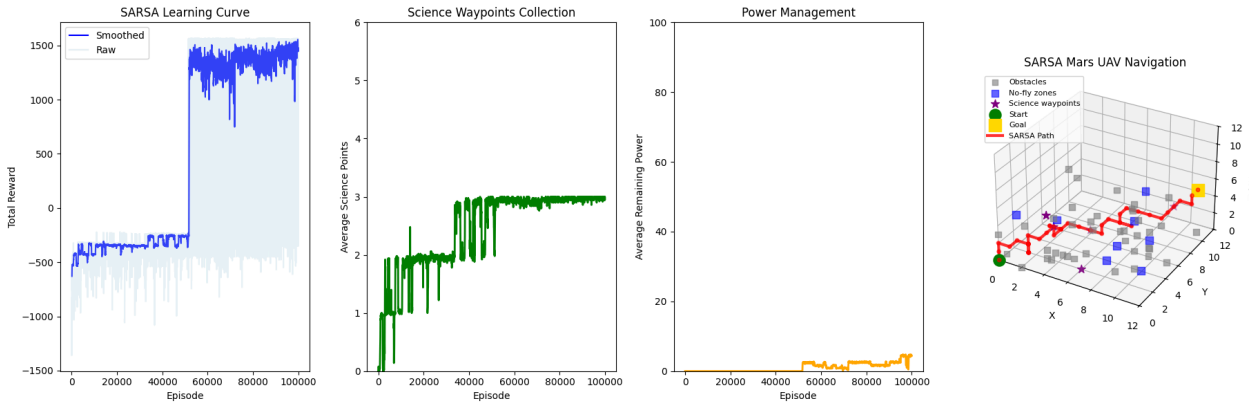

Fig. 8. The learning curve (total reward vs. episode), science waypoints collected, power management graphed per episode, and an example path planned by SARSA [12, 13, 14].

Design

Aeronautics

The aeronautical design of MANTA is a key part of its function. All of these design details are based on testing done in the results & analysis section with these simulations being often referenced throughout the entire design portion of this report. The vehicle will have a mass of roughly 300 kg with approximately 20 kg in payload capacity. Although this report does not cover the precise weight allowances of the vehicle, these are close estimates based on the energy system, material composition, sensors, propellers, and other aspects' weight. MANTA has a forward flight cruising speed of 60 $\frac{m}{s}$ and a VTOL speed of 5 $\frac{m}{s}$. The drag coefficient (Cd) was set at 0.18.

As far as wing specifications go, they were designed to mimic a sailplane's planform. The key feature is the ultra high aspect ratio wings. At lower speeds and low Reynolds number, induced drag is the predominant cause of drag. Since the induced drag scales inversely with the aspect ratio, this wing planform in conjunction with the wingtips was designed to reduce the induced drag. Additionally, due to the lower martian gravity, the bending moment is reduced and an ultrahigh aspect ratio wing becomes more feasible [19]. For these reasons, and those discussed in the results & analysis section, the NACA 5502 airfoil was selected. In addition to the airfoil, the wingspan of the UAV is going to be 13.8 meters with an aspect ratio (AR) of ~25 and a lift coefficient (Cl) of 2.

The MANTA Explorer's rotor configuration was based on a mathematical efficiency model (as seen in figure 3) that compared thrust to power consumption while accounting for the minimum rotor diameter needed for the number of rotors desired. With these models, it was determined that 12 rotors with 1.9 m diameters would work the best for this UAV and would meet at a middle ground between flight stability, energy efficiency, weight, and rotor diameter. Of these, 4 will stay locked in a parallel position to the ground and the other 8 will be able to articulate to become perpendicular with the ground for fixed-wing flight. The 4 static propellers are located in the back and add stability during VTOL. This system is visualized in figures 9 and 10. The rotors are each going to have 2 blades and are designed with a similar cambered and overall airfoil to the Ingenuity propellers [1]. The rotors will weigh 53.7 g each for a total of 644 g (figure 2). The motors for the propellers will each weigh ~750 g and the total rotor configuration will weigh ~9.86 kg. The rotors will spin at 3300-3700 rpm. This spin rate will change depending on the atmospheric density, weather, and maneuvers being performed. The front rotors will be able to tilt using the pictured tilt rotor VTOL mechanism in figures 9 and 10.

In order to better visualize the MANTA Explorer, the Onshape computer aided design (CAD) software was used to create figure 9 [20]. This model is a rough representation of what the concept would look like in the real world and may not be completely accurate to other aspects of the design. The wingspan of this model is 13.8 m, the length of the fuselage is 3.9 m, and the width of the fuselage (at widest section) is 0.3 m.

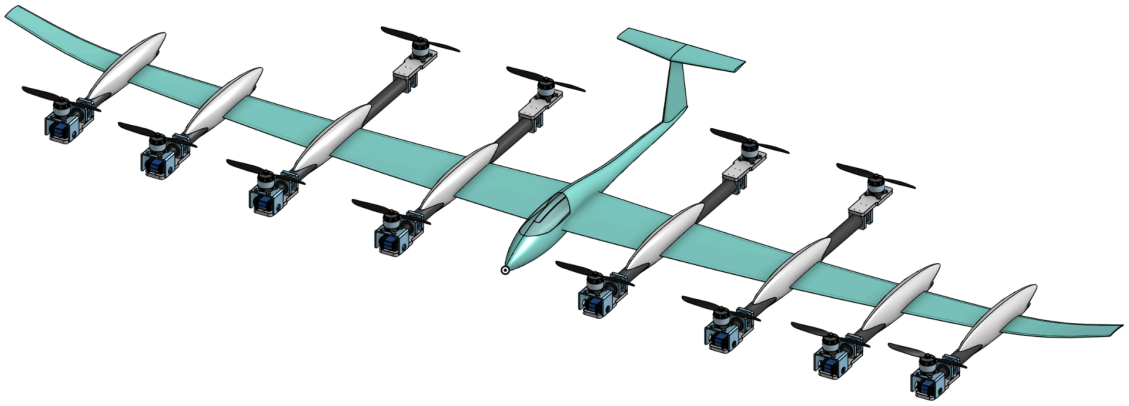

Fig. 9. MANTA CAD made in Onshape [20].

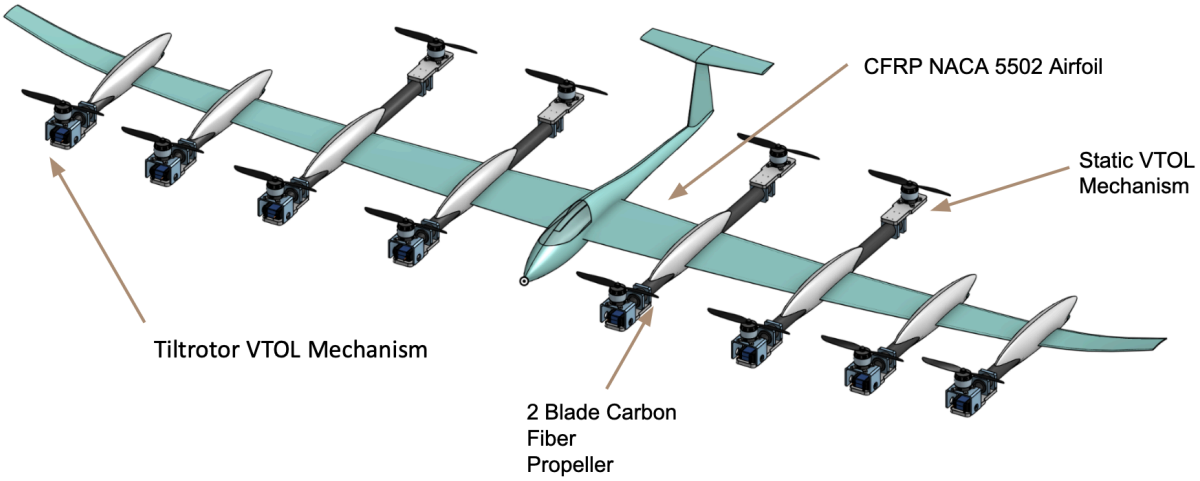

Fig. 10. Annotated version of CAD model from figure 9 [20].

These aeronautical specifications are meant to give a picture of what MANTA will look like and how it will fly in the Martian atmosphere, but there is a significant amount of further research required to determine additional qualities of this design and more specifics of how it will fly and operate in this environment.

Power Supply & Consumption

For any NASA mission, determining the power source is a key part of the vehicle's design. In the case of this mission concept, a number of potential sources

were determined ranging from solar panels to nuclear batteries. In the end it became clear that the best options were either a Multi-Mission Radioisotope Thermoelectric Generator (MMRTG) or solar panels supplemented with Radioisotope Heating Units (RHU) [21, 22]. Both of these offer unique advantages and disadvantages and, therefore, each will be presented as a viable solution with the ideal scenarios of use being described.

Nuclear batteries have been used since the dawn of space flight with the MMRTG being the most recent version that has been or will be used on Curiosity, Perseverance, and Dragonfly [21, 22]. RTGs work by converting the heat made by the radioactive decay of plutonium-238 into electrical energy [22]. Although a different type of nuclear battery– the General Purpose Heat Source- Radioisotope Thermoelectric Generator (GPHS-RTG)– was considered for this concept for its 300 W power output, the MMRTG was chosen despite its lower 110 W output [21, 22]. This is because the GPHS-RTG is an older model, not being produced for two decades, and it does not have the same history of terrestrial missions as the MMRTG [23]. This MMRTG is also incredibly reliable and has a predictable energy output throughout its entire lifespan, providing 14 years of energy at levels that allow for full mission capabilities with potential further use of the nuclear battery past this 14 year point at reduced energy consumption levels. In addition to this electrical energy, the MMRTG produces 2200 W of thermal energy [21]. This heat from the radioactive decay can be channeled around the concept to keep all of its systems warm with the rover itself only having to put in an estimated 5 Wh of usable electricity to power its heaters. This perk of the Radioisotope Power System (RPS) works in Perseverance by using a Rover Heat Rejection System (RHRS) that circulates fluid, specifically CFC-11, through a Mechanically Pumped Fluid Loop (MPFL) that distributes heat throughout the vehicle [24, 25]. A similar system to this would be employed on this concept. RTGs are best used in places where energy from the sun is lacking or inconsistent because they provide constant energy output despite external factors like weather or time of day. They are well suited for Mars since light levels at the surface vary throughout the year and from weather events, but, as a base line, the maximum solar irradiance on Mars is 586 $\frac{W}{m^2}$, close to half of Earth's

value [26]. This risk of failing to receive enough solar power is one of the reasons MMRTGs are more enticing for missions to Mars and they could allow vehicles to travel more freely during the Martian winters and complete long duration missions in the polar regions. A downside of the RPS is that although its power supply is constant, it isn't as energy dense as solar and other systems meaning that it takes a considerable amount of time to store enough power to fly as can be seen in table I. Along with this, a MMRTG costs on average $119 million and it takes the U.S. 3.2 years to create enough of the required plutonium-238 [25, 27]. These limitations should be considered thoroughly and they are the main reason the MMRTG is not being outright recommended as the concept's power source.

When considering solar panels as a potential energy source, it was quickly realized that the high energy requirements of fixed-wing flight and VTOL would be too much if the electrical energy being produced also had to heat the vehicle. For this reason, the solar panel-based design will be heated by RHUs spread throughout the design. These small nuclear batteries are the size of a standard C-cell battery (33 mm tall and 25 mm in diameter) and generate 1 W of thermal energy each [29]. In this design, there will be ~212 RHUs that each weigh 40 g for a total weight of ~8.48 kg. Each of these devices costs an estimated $59,000 for a total cost of ~$12,508,000 and it would take the U.S. ~4 months to create the required amount of plutonium-238 [31] . When considering the solar power aspect of this design, the panels will have a density of 2.5 $\frac{kg}{m^2}$ and a power output of 175.8 $\frac{W}{m^2}$ (30% efficiency) based on the Ingenuity helicopter [26, 31]. Solar panels are ideal when there's access to consistent, unobscured sunlight throughout the mission. On Mars, this means being near the equator and operating during the Martian summer; however, these conditions also tend to form dust storms. Even though newer solar panels on vehicles are resistant to dust storms, the vehicle has to still perform temporary stops to conserve energy. (It should be noted that dust storms on Mars span from the planet's surface up to 40 km in the atmosphere, meaning our vehicle couldn't simply fly above the weather event [7, 32]). Since this vehicle can fly, dust build up shouldn't be a problem since a short flight would blow off any particles obscuring the panels. Overall, solar panels will work as a power

source for this aircraft, but the flight planning process would be more intensive and season dependent than if the MMRTG was used.

As can be seen in table I, both power sources will use lithium-ion batteries because of their reliability and previous use on the planet. The batteries will have an energy density of 250 $\frac{Wh}{kg}$ and, it will be assumed that for these calculations, all systems, unless mentioned otherwise, will have an 80% efficiency [33]. The batteries' weights were calculated based on the following equation that adds an additional 20 kg in assumed casing and electronics weight: $m = (E \cdot U) + 20$. This concept will travel at the described 60 $\frac{m}{s}$ while in fixed-wing flight and the estimated power draws will be found using $E = D \cdot V$. When considering VTOL flight, it is assumed that this maneuvering will last 2 minutes in total and travel at 5 $\frac{m}{s}$ using the described rotor dimensions from the previous section and the equation $E = F \cdot V \cdot \frac{t}{60}$. Apart from these equations, most of the calculations are pretty straight forward and involve simple manipulations of the given values.

Table I		
Comparing MMRTG and Solar with RHU Heating as Potential Power Sources		
	MMRTG	Solar with RHU Heating
	Battery Requirements Comparison	
Power Generator Weight	45.0 kg	51.8 kg
Battery Size	31.25 kWh	31.25 kWh
Battery Capacity	25.0 kWh	25.0 kWh
Peak Power Output	9.08 kW	9.14 kW
Battery Weight	145 kg	145 kg
RHU Weight		~8.48 kg
Total Energy System's Weight	190.00 kg	~205.28 kg
	Power Logistics for Flight Comparison	
Power for Fixed-Wing Flight	9.080 kWh	9.143 kWh
Power for VTOL Flight	231.9 W	234.0 W
Power Output per Sol	2.75 kW	~21.86 kW (under perfect conditions)
Power Output Reliability	Very Consistent	Dependant on Environmental Factors
Time it Takes to Charge to Capacity	9.09 Sols	~1.14 Sols
Maximum Flight Duration	2.50 Hrs	~4.31 Hrs
Maximum Flight Distance	539.12 km	~931.26 km

Table I compares the MMRTG and solar panels as potential power source options for MANTA. Here the battery requirements and power logistics are contrasted between the two options. [21]

As can be seen in table I, the first section, battery requirements comparison, has near identical values across MMRTG and solar power with little variance in battery capacity, specifications, or weight. This is contrasted by the second section, power logistics for flight comparison, where, despite similar power requirements for both fixed-wing and VTOL flight, solar power hits its power capacity, and thus the maximum

flight duration and distance, nearly 8 times faster than MMRTG. This means that a solar powered version of this concept could be ready to fly after around just 7 hours of direct sunlight while a nuclear battery powered version would take closer to 10 sols to meet similar marks. In addition, the solar panel option offers a maximum range 1.7 times that of the nuclear battery. Both of these power options are viable and would work well for MANTA, but it would depend on a variety of factors to decide if the benefits of solar power outweigh the associated risks even when a much more consistent power source, a nuclear battery, is available. For these reasons, this paper will not limit itself by naming a definitive power source for MANTA.

Materials

The material composition of this concept is straightforward and entirely based on the materials used on previous Mars and NASA missions. It should be noted that a wide variety of materials will be used for this aircraft, but many are only included in smaller amounts in individual components of the vehicle and only the materials used in large quantities will be directly mentioned in this section.

The rotors are going to be composed of a rohacell foam structure (0.075 $\frac{g}{cm^3}$) that's coated in a 0.05 mm thick carbon fiber layer (1.57 $\frac{g}{cm^3}$) to add strength and rigidity [1, 34]. This combination of foam and carbon fiber was used for the two Ingenuity rotors and was chosen for its ability to hold its form at high rotational speeds (2400-2800 rpm) and for its low mass. Since this mission's rotors need the same qualities, using the same material composition made sense [1]. For the body and wings of the aircraft, a combination of aluminum and carbon fiber reinforced polymer (CFRP) will be used. Aluminum has been used as the primary structural material in most vehicles to land on Mars because it has a low density for a metal (2.7 $\frac{g}{cm^3}$) and is able to resist the harsh Martian environment (i.e. corrosion, deformation, rusting, ect.) [35]. CFRP (1.4 $\frac{g}{cm^3}$) has been used in past NASA aircrafts to create ultralight wings and hauls with tensile strength stronger than that of steel (~1500-7000 MPa for CFRP) [34, 36]. These are

ideal qualities for the wing and body of this aircraft and, for those reasons, carbon fiber will be used along with aluminum. The main material that will be used to insulate the vehicle internally is polymer-based aerogel that has a low density (0.0011 $\frac{g}{cm^3}$) and is very porous, allowing for high thermal conductivity [37].

Scientific & Navigation Instruments

A selection of scientific instruments, specifically certain kinds of sensors, will be used on the MANTA Explorer in order to collect data to better understand the soil, water, and atmospheric conditions of diverse regions of Mars. Among these instruments is the Laser-Induced Breakdown Spectroscopy (LIBS) that detects any trace compounds in Martian soil or rocks, which could manifest in a number of chemical and biological ways, such as in the form of heavy metal. This instrument was used on the Curiosity rover as part of the Chemistry & Camera (ChemCam) system. LIBS works by firing a laser using a camera and telescope, aiming at a specific soil patch and vaporizing it. The laser beams are rapid-fire; about thirty beams are shot at each particular point. The resulting emission spectra is analyzed by a spectrometer situated inside the vehicle to determine the elemental makeup of the object. In order to collect the most accurate data possible, laser beams are shot at multiple different points, and the data collected from said points will be averaged [38, 39].

An Ion Sensitive Field Effect Transistor (ISFET) sensor will be used to collect data on water on Mars, due to its fast response time in determining pH. The transistor's gate is made of a pH-sensitive material, which, when making contact with the substance that is under observance, generates a charge due to the hydrogen ions interacting with it. The voltage measured from this charge once it creates a conductivity difference inside the transistor is then used as the pH value, as the two values are proportional. Some of the benefits that come from using this instrument are its relatively small, portable size, and its ability to very accurately measure pH in any temperature and harsh environments, as electrode damage isn't a concern with this durable tool [40]. In tandem with ISFET, the Dynamic Albedo of Neutrons (DAN) sensor will work to identify trace concentrations of water in nearby minerals in quantities as low as 0.1%. This

system works by looking at neutron radiation of trace amounts of water up to 1 meter below the ground [39].

For atmospheric sampling, a TLS (Tunable Laser Spectrometer) will be used to detect certain trace gases, just as it was successfully used on the Curiosity rover. Inside the body of the spectrometer is a chamber (the Herriott cell), in which a laser beam of a specific wavelength is fired at the gas sample under observation, passing through it in a back-and-forth manner with the help of mirrors inside the chamber. The light absorption is then measured, and the spectrometer further aids in detecting and quantitatively measuring trace gases in the Martian atmosphere, such as carbon dioxide, water vapor, and methane [41].

Additionally, Vaisala models of HUMICAP and BAROCAP sensors will be employed for even further, in depth study of the Martian atmosphere. The HUMICAP will aid in observing Mars' water vapor exchange in the atmosphere by gathering information about humidity. The body of the sensor is essentially made up of a polymer film that is very moisture-sensitive and situated between two electrodes. Humidity changes are tracked as the film absorbs or releases water (depending on how exactly the humidity is changing), and the resulting change in capacitance is picked up by the sensor and is in turn used as the final humidity measurement [42]. The BAROCAP will measure and track atmospheric pressure changes through the interpretation of temperature data. The inside of the sensor is made up of a small vacuum that is encased by a silicon membrane, which contracts and expands in response to pressure increase and decrease. The two opposite electrodes (one acting as each side of the vacuum gap) get closer and further from each other depending on the fashion in which the membrane bends, altering the capacitance. The capacitance measurement is then used for the final pressure reading [43].

The final sensor is the Mars Environmental Dynamics Analyzer (MEDA) that will focus on gathering weather data, including predicting the formation of dust storms. MEDA was employed on Perseverance and would be of particular value to this mission concept since this will be the first mission to be able to record detailed data over an

extended period about the unique atmospheric composition of different altitudes on Mars [44].

In addition to these scientific instruments, the MANTA Explorer will also use a variety of navigational instruments to aid in flight and flight planning. The same type of Navigational Cameras (NavCam) used in Ingenuity and Perseverance will be used for this concept. These cameras provide black and white video that is not sent back to Earth and instead is only used for navigational purposes. In order for the NavCams to have an unobscured field of view (FoV), which is required for difficult VTOL maneuvers, two cameras per a side of the vehicle are needed [45]. A total of 10 NavCams will be used (2 front side, 2 back side, 2 left side, 2 right side, 2 bottom) with each of them weighing 200 g [46]. These NavCams each have an FoV of 67º and the pairs will be angled either 14º or 22º away from each other. This is in order to reduce the size of any blind spots not in the immediate vicinity of the aircraft [47]. The placement of these NavCams is shown in figure 11 from a top view of the fuselage. The total area of the blind spots is 8.526 m^2 and MANTA has an unobstructed FoV after a maximum 2.99 m distance from its fuselage. Although these blind spots could be eliminated with the addition of more NavCams, each camera adds significant weight to the aircraft so it would be best to use the configuration seen below.

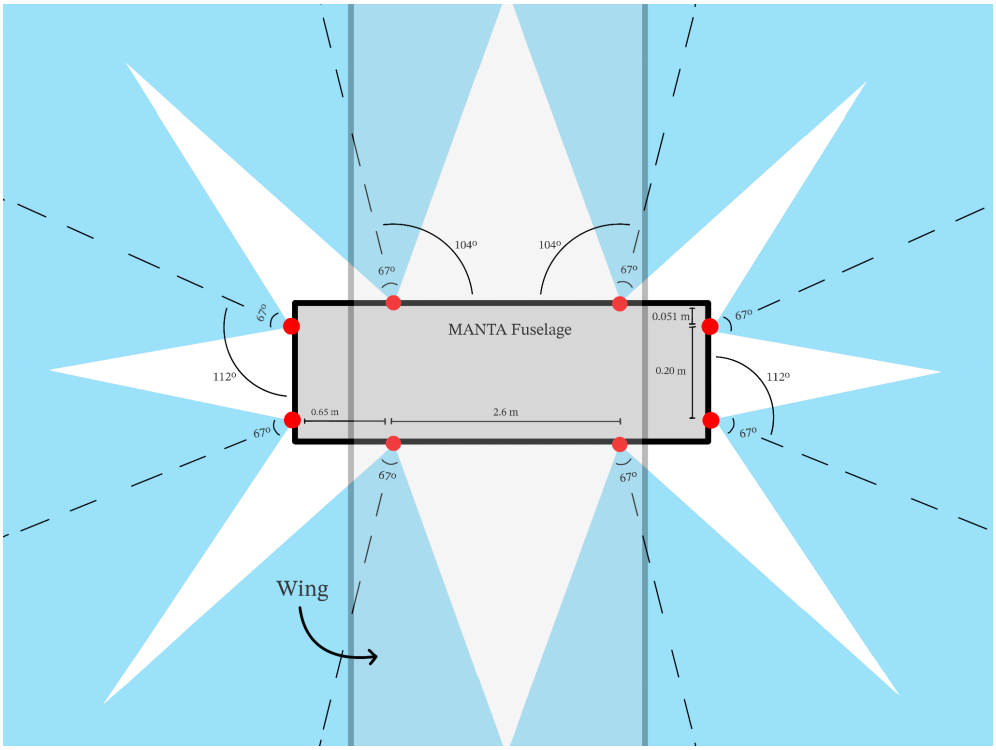

Fig. 11. This is a top view depiction of the FoV of MANTA using its NavCams. This illustration is not to scale with angles, distances, and shapes being distorted and/or simplified. The red dots represent NavCams with 2 on the underside of the vehicle not being shown. The blue region represents areas visible to the aircraft (extends well beyond what is depicted) and the white areas are blindspots of the system. The grey areas represent the UAV fuselage and wing. The dashed lines are the medial lines of the cameras. This depiction's measurements are symmetrical and it should be assumed that if an angle or distance is shown on one side of the fuselage, it is identical on the opposite side.

The second type of navigational instrument is the Return to Earth (RTE) camera that weighs 40 g. This device records colored video that is sent back to Earth to allow for well informed flight planning. There will be 4 of these RTE cameras (1 back side, 1 left wing, 1 right wing, 1 bottom) and with a 133º FoV, they do not need to be specially angled [48]. The final navigation camera is the Mastcam-z. This camera system, employed on Perseverance, provides high resolution, 3D photos and could be used for flight planning and scientific purposes. There will be 2 of these cameras mounted on the front of the UAV with a combined weight of 4 kg [44]. In addition to these cameras, Light

Detection And Ranging (LiDAR) will be used to aid in VTOL landing and to help with mapping of terrain MANTA flies over. The total weight for the cameras is 6.16 kg and the LiDAR system weighs an additional 4 kg [49]. Apart from these spectrometers, environmental data, like wind speed and dust storm formation, will be recorded by the aforementioned MEDA system and internal devices associated with the primary computer will also aid in autonomous flight [44].

Software

MANTA will use a variety of AI and ML applications to aid in flight, VTOL, and other aspects of its mission. In this section, the models and simulations from the results & analysis are explored further in relation to how they are designed to function in tandem with the mechanical and scientific functions of this UAV.

To start off, there are many things that the path planning algorithm needs to take into account. To follow is an overview of the inputs it will need to factor in. Orbital maps from Mars orbiters like the Mars Reconnaissance Orbiter (MRO) provide large-scale terrain information. This will provide Digital Elevation Models (DEMs), which reveal the topography of the landscape; slope and aspect analysis provide the steepness of the terrain, which helps find areas that may be unsafe for low-altitude flight or landing; surface roughness and rock abundance [50]. Onboard sensors provide a clearer real-time terrain view. LiDAR is a way to measure distances to the ground and objects, which helps detect sudden elevation changes. Stereo/Monocular cameras (part of the NavCam system) get images to recreate 3D surfaces using computer vision. Stereo cameras collect the depth and surface texture, while monocular cameras are helpful for terrain classification when paired with AI algorithms [45, 49].

Autonomous terrain classification is a key requirement for MANTA's mission on Mars. It allows for safe path planning, hazard avoidance, and scientific site selection. Convolutional Neural Networks (CNNs) allow for robust, automated extraction and classification of these features by training on labeled image datasets [51]. Understanding the terrain helps determine the ideal landing place and scientific waypoints for the UAV. The data will come from the onboard NavCams.

CNNs are a type of deep learning model that works well for processing and understanding image data, for tasks like image classification. CNNs preserve the spatial

layout of an image, which allows them to recognize specific patterns and the locations of those patterns [52]. The core architecture of CNNs is based on several different types of layers, each one taking in more abstract information from the previous one.

The convolutional layers are the fundamental part that extracts features such as edges, texture, and shapes from images. It involved sliding a filter (kernel) (K), which is a small matrix of weights, over the input image (I). At each part, it computes the dot product of the filter values and the pixel values, outputting this all into a feature map (S) where each element $S(i,j)$ represents the intensity of a feature that the kernel detected at a specific position. The filter's weights are learned during training in order to detect specific features. At each convolutional layer, multiple different filters are applied.

$$S(i,j) = (I * K)(i,j) = \Sigma m \, \Sigma n \, I(i - m, j - n)K(m,n)$$

Here, I is the input image, K is the kernel, (i,j) are the coordinates on the feature map, and (m,n) are the coordinates in the kernel. Stride (S) specifies the number of pixels by which the filter moves across the input image or feature map in each step.

The pooling layers are after the convolutional layers, and it helps keep only the essential information. There is max pooling (taking the highest value in a region) and average pooling (taking the average value in a region). The fully connected layer is where all the neurons are connected, it performs classification using the features extracted by previous layers. It can use softmax to make the probability for different classes for a test image. However, one of the main constraints of the terrain classification approach is the lack of data from a UAV's point of view of Mars terrain. One way to go around this is by converting existing image data from past rovers' missions on Mars to images that look like an aircraft's point of view using synthetic data generation.

After terrain classification, a hazard map will be created to help with MANTA's navigation, landing and scientific exploration. The surface images will be split into regions using superpixels, grouping pixels will have similar properties like texture and elevation [53]. These will then be assigned to a terrain class such as "crater", "plain",

“dune”, “steep slope”, ect. [54]. Advanced deep learning approaches such as NOAH-H are able to classify even more specific classes such as “bright dune” or “impact ejecta” [55]. For MANTA, the terrain classes will be things like: plains, crater material, steep slopes, bedrock, impact ejecta.

Each classified terrain patch will receive a hazard score based on a weighted sum of risk features.

$$H_p = \sum_{i=1}^{n} w_i F_{i,p}$$

$F_{i,p}$ is the values of the i-th risk factor (slope, rock abundance, surface roughness) for patch p and w_i is a weight that shows how important that risk factor is to the cost [56]. Terrain patches classified as “steep slope” or “rock field” will generally have higher hazard scores, showing riskier regions for landing, while “plains” or “smooth bedrock” patches will generally have lower hazard scores, making them more favorable. As new imagery is acquired from the NavCams, MANTA will constantly update the hazard scores. This can then be integrated with the reinforcement learning (RL) path planning algorithm discussed later, where lower hazard scores are favored and higher hazard scores are penalized.

To look into the atmospheric conditions, the atmospheric sensors will measure wind speed/direction, temperature, pressure, and dust particle concentration using the MEDA, HUMICAP, and BAROCAP systems. These onboard sensors and orbital weather data will help the path planner avoid hazardous weather zones.

The vehicle’s battery and power consumption will be monitored to make sure the planned routes are feasible. The sensor battery levels will also play a role. The UAV payload, maximum altitude, and speed limits will help plan paths. The mission parameters, such as scientific points of high interest, will affect the planner as well.

MANTA will use reinforcement learning for its path planning. Reinforcement learning is a branch of machine learning where an agent learns to make decisions by interacting with its environment and receiving feedback in the form of rewards or penalties. The agent’s goal is to maximize its long-term rewards by learning which

actions lead to the best outcomes [54]. In this case, the agent will be the vehicle. Below, figure 12, is a representation of the Markov Decision Process (MDP), which is how the agent and environment communicate with each other. The three main components are the state, action, and reward.

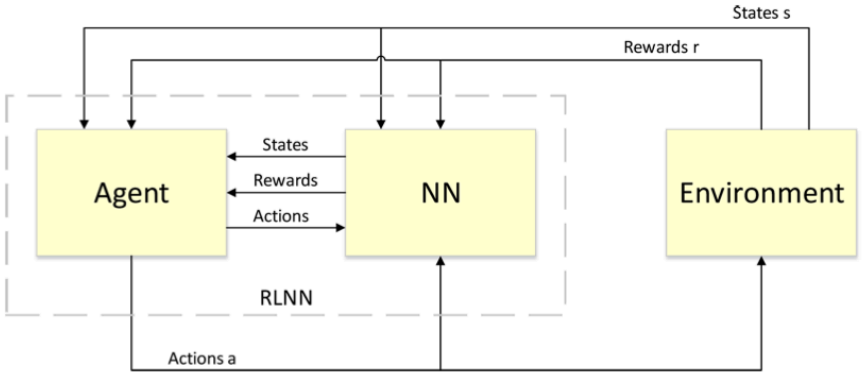

Fig. 12. Markov Decision Process (MDP) [57].

A key characteristic of MDPs is the Markov Property. This means that the next state transition is only related to the current state. The current state contains all the necessary information from the past states, making it possible to predict the future state solely based on the present state.

The Q-learning algorithm aims to maximize overall long-term rewards and can find optimal paths. It creates and constantly updates the Q-table, which stores Q-values, that represent the expected maximum reward value for each possible action that the agent can take in each given state. The Q-learning updates the Q-value using the new reward and original Q-value, in a process called value iteration. Below is the equation used to update the Q-values over time.

$$Q_{new}(s_t, a_t): (1 - \alpha) \times Q(s_t, a_t) + \alpha \times (rt + \gamma \times max_a Q(s_t + 1, a))$$

rt is the immediate reward from moving from St to St+1. α (learning rate) is a value between 0 and 1 which determines how much new information overrides the old information. γ (discount factor) is a value between 0 and 1 which determines the

importance of future rewards, a larger γ means that the agent pays more attention to long-term rewards. $max_a\ Q(st\ +\ 1, a)$ is the maximum Q-value among all possible actions (a) in the next state ($st\ +\ 1$) [13, 14, 15].

The action policy is how the agent chooses actions during exploration, it uses an ε-greedy policy. This means that the agent will most likely choose the action with the highest Q-value, however there is the probability of ε that the agent will randomly choose a different action, which gives the agent the opportunity to explore parts of the environment it might otherwise ignore [58]. This is different from the evaluation/update policy, which updates the Q-values, because it always chooses the action with the maximum Q-value.

The Q-learning algorithms use reward and punishment rules to guide the learning process. In this study's experiments, they found that the Q-learning algorithm can reduce computation time by 50% and shorten the path length by 30% compared to the SARSA algorithm. For more complex problems, like obstacle avoidance, a neural network can be used to estimate Q-values, this is called DQN. For this case, it would be useful for reaction to dynamic or previously unmapped obstacles on the terrain [13, 14, 15].

The reward function for MANTA penalizes each step, penalizes even more for "gray blocks", which are the obstacles, and gives a high reward for reaching the goal. Positive rewards would include reaching scientific waypoints, conserving power through shorter paths, and completing data collection tasks. Punishments would be for colliding with bad terrain, entering "no-fly zones" (places with hazards), and excessive energy consumption. The ε-greedy policy will ensure that the agent will randomly explore new places, making sure that the Mars UAV can find optimal paths in places with unknown terrain or unexpected environmental conditions [13, 14, 15, 58].

A simple approach was taken to demonstrate the basic Q-learning algorithm. The results are presented in the results & analysis section. Next, a more realistic approach was taken to represent the real Mars environment, including the terrain and atmospheric conditions to train a deep Q-learning algorithm that had a neural network, shown also in the results & analysis. This can be seen in figure 8 [13, 14, 15].

DQN is different from the Q-learning algorithm because the agent is implemented as a neural network that takes the current state and outputs the Q-values for each

possible action [50]. The network is trained based on experience replay, state-action-reward-next_state-done transitions are stored and the neural network learns to minimize the difference between predicted and actual future rewards (based on the Bellman equation). This can be seen in figure 7 [13, 14, 15].

The other reinforcement learning algorithm is called SARSA, which is an on-policy algorithm [58]. As can be seen in figure 8, being on-policy means that it updates its Q-values based on the actual action that the agent takes. This is different from off-policy algorithms like a DQN, which means that it assumes that the agent took the most optimal action, even if it didn't [57]. The main parts of the SARSA algorithm are the state (current position in the environment), action (movement of the agent), reward (the feedback of that action), next state (the state after taking the action) and the next action (the action in the next state based on the current policy). The following equation is how SARSA updates the q-values:

$$Q(s_t, a_t): Q(s_t, a_t) + \alpha[r_{t+1} + \gamma Q(s_{t+1}, a_{t+1}) - Q(s_t, a_t)]$$

$Q(s_t, a_t)$ is the Q-value for that state-action pair as of the current moment at step t, α is the learning rate which represents by how much the Q-values change, r_{t+1} is the reward for action a_t in state s_t, γ represents how important future rewards are, and $Q(s_{t+1}, a_{t+1})$ represents the Q-value for the $t + 1$ state-action pair [13, 14, 15].

For scheduling, CASPER (Continuous Activity Scheduling Planning Execution and Replanning) will be used; it uses AI for scheduling and planning. It automatically responds to events and replans the schedule as deemed necessary. It generates mission operation plans based on goals from the onboard science module. It takes into account operations and resource constraints as well. CASPER will have to be modified to fit MANTA's needs [59].

In order to safely land on Mars' surface, MANTA will use a Linear-Quadratic-Regulator (LQR) after precomputing the optimal path for a safe landing [60, 61]. Before beginning the landing algorithm, MANTA must pick a safe

landing area using the hazard map described earlier. MANTA will use 2 matrices that represent the current "state" of the UAV: the first one, x, will be a 12-dimensional state vector (in the order $x,\ y,\ z,\ v_x,\ v_y,\ v_z,\ \phi,\ \theta,\ \Psi,\ v_\phi,\ v_\theta,\ v_\Psi$ where ϕ, θ, and Ψ are the roll pitch and yaw respectively) that contains the cartesian and angular positions and velocities of MANTA in all three dimensions [62]. Additionally, there will also be u, a 4-dimensional state vector that contains the total thrust, roll, pitch and yaw of the UAV. First, in order to compute the optimal trajectory, we will minimize the following cost function:

$$\int_0^T (x^T W x \ + \ u^T R u)\, dt \ + x^T(T) P_1 x(T)$$

T is the total time of the landing, x^T and u^T are the transpose of x and u, respectively, W is a $12 \ \times 12$ state weighting matrix, R is a $4 \ \times \ 4$ control weighting matrix, and P_1 is a terminal cost weight matrix. The term outside of the integral, the "terminal cost", penalizes the UAV for landing away from the desired landing area, while the "running cost" inside the integral will add cost based on its actions during the landing process. P_1, Q, and R will be predefined and tuned through simulation and testing in a Mars-like environment. Minimizing this cost function will result in a smooth descent with moderate thrust, as the quadratic expression inside the integral will discourage sudden large amounts of thrust. To actually minimize this integral, we can use Hermite-Simpson collocation to turn the optimization problem into a nonlinear program, and then we can solve the nonlinear program with an Interior Point Optimizer (IPOPT) [63]. Next, we will use LQR to make sure the UAV maintains this trajectory as accurately as possible during the landing. If we had an infinite flight path, we would want to minimize this function:

$$\int_0^T (\delta x^T W \delta x \ + \ \delta u^T R \delta u)\, dt$$

δx and δu are the deviation of the UAV's position/velocity and thrust from the precomputed trajectory. However, we want the UAV to land in the intended position, so we will add a second term containing the UAV's final position's deviation from that state, giving us:

$$\int_0^T (\delta x^T W \delta x \ + \ \delta u^T R \delta u)\, dt \ + \ \delta x^T(T) P_1 \delta x(T)$$

Again, new values of W, R, and P_1 will be predefined and tuned based on simulation and testing in a Mars-like environment. The method for minimizing this is to solve the time-varying Riccati equation backward from the time of landing, and use this to correct deviations from the original flight plan in real time [63]. This will give us a gain matrix K, and at any given time t we can apply control $u(t) \ = \ K(t)\delta x(t)$ in order to accurately follow the desired path. Finally, the LQR algorithm only calculated the amount of thrust and rotation of the UAV, but we need to translate that into thrusts of the individual rotors, which we can do with a motor-mixing algorithm.

Mission Goals

The goal of the MANTA mission is to deepen our understanding of the Martian environment and its chemical composition at the atmospheric, surface, and subterranean levels over large regions of the planet while demonstrating new technology capabilities on Mars. The scientific goals of this mission include creating detailed maps of the Martian terrain, investigating the planet's atmosphere at different altitudes, and searching for distinct signs of water. The range of this aircraft will allow it to collect data from diverse and distant locations on Mars at a far greater scale than a rover could achieve and with more precision than current orbiters. As is described in the scientific and navigation instruments section, LiDAR technology will be used in flight, in combination with images taken by the RTE cameras, to create detailed maps that will

help inform the UAV where to land, where to send future autonomous missions, and where future manned missions could visit or be located. This technology will improve upon the existing maps created by the MRO while incorporating a third dimensional aspect that will allow for the detailed visual and chemical analysis of the multitude of the different cliffs, hills sides, crater edges, and lake basins that were previously not visible to orbiters [64].

When trying to better understand the atmospheric conditions and related weather patterns of Mars, it must be stated that although this topic has been studied in depth at elevations where rovers and landers have been sent, limited data has been collected at altitudes above -1828 meters relative to the zero elevation-level as is defined by measurements from MOLA and the Areoid model. To better understand -1828 meters in this context it should be noted that, defining elevation on Mars is tricky since there's no sea level for it to be based on, meaning the zero-elevation level of the planet is actually at a relatively high altitude. This explains why, especially when compared to the craters, vallies, and depressions rovers and landers are usually sent to, the maximum height that any terrestrial mission has reached on the ground is a negative number [24, 64, 65]. These limited data points above -1828 meters primarily consist of temperature and pressure reading taken as various vehicle capsules descended through the Martian atmosphere [64]. For this reason, having the ability to conduct atmospheric research at varying elevation for extended periods of time is imperative to better understanding weather patterns, temperature fluctuations, wind speeds, and other meteorological phenomena occurring on Mars. By far the most disruptive type of these phenomena is the Martian dust storm. Despite their assumed menacing nature, dust storms on Mars are only a threat because they can obscure the sun and thus limit the power output of solar panels and they can interfere with visual-based navigational systems such as Sky Crane [7, 64]. In the same fashion to how cold and warm fronts form on Earth, Mars has similar patterns in which warm air rises near and around the equator, where Hadley Cells are present, then circulates northward and southward, cooling off in the process. On Mars, these cells and fronts are much more distinct and have a "sharp" border where temperature and pressure shift dramatically over a short distance [66]. The rising warm air at the borders of these weather patterns carries dust particles up into the atmosphere where they can accumulate and form large dust storms that last for days to

months and can reach 30 to 40 kilometers high [7]. Since dust storms form in warmer conditions, they often occur during the Martian summers which are roughly twice as long as on Earth. This effect is exacerbated in the southern hemisphere where it gets warmer because of the elliptical orbit of the planet [9]. Utilizing the aforementioned MEDA environmental sensor system, along with the HUMICAP and BAROCAP, both while in flight and while stationary will be a key mission goal for this vehicle and will, hopefully, help to shed light on the specifics of how dust storms form and what are the factors that define the intensity and scale of the event [44].

In addition to mapping terrain and its other uses aboard Curiosity and Perseverance, spectroscopy also serves to identify compounds only created in the presence of water or life. Particular the further detection of high levels of methane (CH_4) would continue to be a strong signal for biological offgassing [67]. The DAN, ISFET, LIBS, and TLS systems would specifically look for water and trace compounds through direct and indirect signs. The LIBS and TLS would use emission spectra to look for the various trace compounds in rocks and soil while DAN and ISFET would aim to identify water trapped in ice or minerals [38, 39]. It has been widely hypothesized that Mars was once covered in water-rich oceans; directly discovering the remnants of these oceans in the form of large frozen or liquid water reservoirs underground would revolutionize the field of planetary science and, possibly, pave the way for the discovery of Martian life [68]. For these reasons, the search for water will be a top mission goal for MANTA and it will fully employ the DAN and ISFET systems to further this goal.

The primary technical goal of MANTA is to prove fixed-wing flight is feasible in the Martian atmosphere. The use of an airfoil designed for low Reynolds numbers allows MANTA to generate lift in Mars' thin atmosphere. This, along with the VTOL rotor configuration detailed in the aeronautics section, will allow the aircraft to perform take-offs and landings in locations identified through in-flight mapping. The use of solar panels and RHUs or a MMRTG would provide MANTA with a large range, a feature valuable in completing scientific research. All of these technical areas will be aided by the AI/ML applications as are detailed in the software section. Similar AI software has been used on Mars before, most notably in CASPER on Perseverance, but MANTA will

rely more on these programs than any previous mission. When Ingenuity made its historic flights, it showed the potential of aerial vehicles in planetary exploration. By proving fixed-wing flight is possible on Mars, MANTA would pave the way for the future of extraterrestrial exploration.

Conclusion & Recommendations

After conducting research, performing simulations, and designing, the MANTA Explorer concept has been shown to be a viable solution to the described wicked problem. It employs innovative technical solutions that allow it to more effectively explore large areas of Mars while collecting unprecedented quantities of qualitative and quantitative data about the geological and atmospheric nature of the planet. From an aviation standpoint this concept will use 12 propellers with 1.9 m diameters to perform VTOL and forward flight in the Martian atmosphere. With a wingspan of 13.8 m and an airfoil optimized for low Reynolds numbers, MANTA will gracefully traverse the planet's landscape while expanding on the technical research done by Ingenuity. To power this flight and the other operations of the UAV, lithium ion batteries will be used with either a MMRTG or solar panels charging the battery. Both of these power source options would be sufficient for extended flight and would allow MANTA to conduct high quality scientific and technical research, but there are associated risks with solar power that may or may not outweigh its benefits when a more consistent power source, a nuclear battery, is available. For these reasons, this report leaves the final question of power source undetermined in order to not limit the design potential of this concept. MANTA will be equipped with a variety of sensors to aid it in smoothly collecting and analyzing data samples pertaining to the mission goals of this vehicle. In addition, the concept will use terrain classification backed by CNNs for hazard mapping. It will also use reinforcement learning to help with path planning, and the CASPER scheduling system. It will also optimize a landing path using Hermite-Simpson collocation and IPOPT, and maintain that path throughout the landing with LQR. This explorer aims to further our understanding of scientific and technical areas of interest and thus the mission goal will revolve around terrain, atmosphere, and geological composition; weather patterns; identifying quantities of water; and fixed-wing/VTOL flight.

Apart from these specifics about the MANTA Explorer's design and mission objectives, there are a number of areas we wish to recommend further research be conducted. As stated in the methods section, this report was written by a small team tackling a large challenge and associated wicked problem. We are only scraping the surface of designing a full mission to Mars with this report. Further examination of forward and VTOL flight mechanisms, rotor airfoil, flap configuration, power consumption, and AI/ML applications would be beneficial technical areas to conduct additional research. From a scientific perspective, a more defined mission goal, expanded set of scientific instruments, and set location on the planet would further help in ironing out the design of this concept.

The development of the Mars Aerial Navigation Terrain & Atmosphere Explorer concept demonstrates the plausibility and distinct benefits of aerial exploration of the Red Planet using a fixed-wing vehicle. Building on the work of Ingenuity, Perseverance, Curiosity, and all past missions to this planet, an UAV like MANTA can unlock a vault of scientific knowledge that will redefine our understanding of Mars and help to usher in a new era of autonomous extraterrestrial exploration– an era centered around flying vehicles.

References

[1] “Ingenuity,” *NASA Jet Propulsion Laboratory (JPL)*, 2020. https://www.jpl.nasa.gov/missions/ingenuity/

[2] Great Barrier Reef Foundation, “Manta Ray Facts,” *Great Barrier Reef Foundation*. https://www.barrierreef.org/the-reef/animals/manta-ray (accessed Jul. 24, 2025).

[3] D. Williams, “Mars Exploration Timeline,” *nssdc.gsfc.nasa.gov*, 2024. https://nssdc.gsfc.nasa.gov/planetary/chronology_mars.html (accessed Jul. 20, 2025).

[4] CoFlow Jet, “Mars Aerial and Ground Global Intelligent Explorer (MAGGIE) - NASA,” *nasa.gov*, Jan. 04, 2024. https://www.nasa.gov/general/mars-aerial-and-ground-global-intelligent-explorer/ (accessed Jul. 20, 2025).

[5] The European Space Agency, “Comparing the atmospheres of Mars and Earth,” *www.esa.int*, Apr. 09, 2018. https://www.esa.int/ESA_Multimedia/Images/2018/04/Comparing_the_atmospheres_of_Mars_and_Earth (accessed Jul. 20, 2025).

[6] NASA, “Mars: Facts - NASA Science,” *science.nasa.gov*, Nov. 20, 2024. https://science.nasa.gov/mars/facts/ (accessed Jul. 20, 2025).

[7] K. Hille, “The Fact and Fiction of Martian Dust Storms,” *NASA*, Sep. 18, 2015. https://www.nasa.gov/solar-system/the-fact-and-fiction-of-martian-dust-storms/ (accessed Jul. 20, 2025).

[8] “Here’s How Curiosity’s Sky Crane Changed the Way NASA Explores Mars - NASA,” *NASA*, Aug. 07, 2024. https://www.nasa.gov/missions/mars-science-laboratory/curiosity-rover/heres-how-curiositys-sky-crane-changed-the-way-nasa-explores-mars/ (accessed Jul. 20, 2025).

[9] Arizona State University, “Atmosphere,” *Mars Education at Arizona State University*, 2019. https://marsed.asu.edu/mep/atmosphere (accessed Jul. 20, 2025).

[10] T. ORMSTON, “Time delay between Mars and Earth,” *Mars Express*, Aug. 05, 2012. https://blogs.esa.int/mex/2012/08/05/time-delay-between-mars-and-earth/ (accessed Jul. 20, 2025).

[11] W. Koning Aerospace, E. Aerospace, and W. Johnson, “Low Reynolds Number Airfoil Evaluation for the Mars Helicopter Rotor,” Jul. 2025. Available: https://rotorcraft.arc.nasa.gov/Publications/files/Koning_Romander_Johnson_Low_Reynolds_Number_Airfoil_Evaluation_FINAL_ARC.pdf
[12] “matplotlib.pyplot — Matplotlib 3.5.3 documentation,” *matplotlib.org*. https://matplotlib.org/3.5.3/api/_as_gen/matplotlib.pyplot.html (accessed Jul. 20, 2025).
[13] “mpl_toolkits.mplot3d.axes3d.Axes3D — Matplotlib 3.3.3 documentation,” *Matplotlib.org*, 2020. https://matplotlib.org/3.3.3/api/_as_gen/mpl_toolkits.mplot3d.axes3d.Axes3D.html (accessed Jul. 20, 2025).
[14] “Astropedia - Mars MGS MOLA - MEX HRSC Blended DEM Global 200m,” *Usgs.gov*, 2018. https://astrogeology.usgs.gov/search/map/mars_mgs_mola_mex_hrsc_blended_dem_global_200m (accessed Jul. 20, 2025).
[15] Google, “Google Colaboratory,” *Google.com*, 2019. https://colab.research.google.com/ (accessed Jul. 20, 2025).
[16] J. Winslow, H. Otsuka, B. Govindarajan, and I. Chopra, “Basic Understanding of Airfoil Characteristics at Low Reynolds Numbers (104–105) | Journal of Aircraft,” *Journal of Aircraft*, vol. 55, no. 3, 2017, doi: https://doi.org/10.2514/ja.2018.55.issue-3;journal:journal:ja;website:website:aiaa-site;wgroup:string:AIAA.
[17] NASA, “NACA Airfoils - NASA,” *NASA*, Jan. 31, 2017. https://www.nasa.gov/image-article/naca-airfoils/ (accessed Jul. 20, 2025).
[18] H. Sutton, “Peter Morgan Sutton,” *BMJ*, vol. 348, no. mar31 11, pp. g2466–g2466, Mar. 2014, doi: https://doi.org/10.1136/bmj.g2466.
[19] J. G. Leishman, “Gliders & Sailplanes,” *eaglepubs.erau.edu*, Jan. 2023, Accessed: Jul. 20, 2025. [Online]. Available: https://eaglepubs.erau.edu/introductiontoaerospaceflightvehicles/chapter/gliders-sailplanes/

[20] OnShape, “Onshape | Product Development Platform,” *www.onshape.com*, 2014. https://www.onshape.com/en/ (accessed Jul. 22, 2025).
[21] NASA, “Multi-Mission Radioisotope Thermoelectric Generator (MMRTG),” 2020. Accessed: Jul. 20, 2025. [Online]. Available: https://mars.nasa.gov/internal_resources/788/
[22] “Radioisotope Power for Fueling Space Missions,” *Stanford.edu*, 2023. http://large.stanford.edu/courses/2023/ph240/dedeler2/ (accessed Jul. 20, 2025).
[23] P. Davis, “Legacy Systems,” *NASA Science*, Feb. 09, 2024. https://science.nasa.gov/planetary-science/programs/radioisotope-power-systems/legacy-systems/ (accessed Jul. 20, 2025).
[24] M. Mahzari *et al.*, “Development and Sizing of the Mars 2020 Thermal Protection System.” Accessed: Jul. 20, 2025. [Online]. Available: https://ntrs.nasa.gov/api/citations/20220006688/downloads/Development%20and%20Sizing%20of%20the%20Mars%202020%20Thermal%20Protection%20System_AIAA%20Aviation%202022.pdf
[25] “National Aeronautics and Space Administration Multi-Mission Radioisotope Thermoelectric Generator (MMRTG),” NASA, May 2019. Accessed: Jul. 20, 2025. [Online]. Available: https://discovery.larc.nasa.gov/PDF_FILES/26_MMRTG_Fact_Sheet_update_5-7-19-Mission_Planner.pdf
[26] D. R. Williams, “Mars Fact Sheet,” *Nasa.gov*, Oct. 03, 2024. https://nssdc.gsfc.nasa.gov/planetary/factsheet/marsfact.html (accessed Jul. 20, 2025).
[27] “Pu-238 shipment quantity ‘opens the tap’ for space missions | ORNL,” *www.ornl.gov*. https://www.ornl.gov/news/pu-238-shipment-quantity-opens-tap-space-missions (accessed Jul. 20, 2025).
[28] A. Tursz, *Les oubliés*. 2010.
[29] “DISCOVERY AO LIGHTWEIGHT RADIOISOTOPE HEATER UNIT (LWRHU) INFORMATION SUMMARY,” *NASA*, Sep. 2009. https://discovery.larc.nasa.gov/PDF_FILES/6RHU_Description.pdf (accessed Jul. 20, 2025).

[30] “DISCOVERY AO RADIOISOTOPE HEATER UNIT (RHU) INFORMATION SUMMARY,” *NASA*, Apr. 2004. https://discovery.larc.nasa.gov/PDF_FILES/LARHU_Descrip_final.pdf

[31] “Mars Helicopter’s Solar Array as Seen by Perseverance’s Mastcam-Z - NASA Science,” *science.nasa.gov*. https://science.nasa.gov/resource/mars-helicopters-solar-array-as-seen-by-perseverances-mastcam-z/ (accessed Jul. 20, 2025).

[32] NASA, “Spirit - NASA Science,” *science.nasa.gov*, Dec. 19, 2024. https://science.nasa.gov/mission/mer-spirit/ (accessed Jul. 20, 2025).

[33] Z. Lin, D. Li, and Y. Zou, “Energy efficiency of lithium-ion batteries: Influential factors and long-term degradation,” *Journal of Energy Storage*, vol. 74, pp. 109386–109386, Dec. 2023, doi: https://doi.org/10.1016/j.est.2023.109386.

[34] “Stories - ARK Carbon blades x TeXtreme,” *Textreme.com*, 2021. https://www.textreme.com/stories/ingenuity (accessed Jul. 20, 2025).

[35] Thyssenkrupp, “Density of Aluminium,” *Materials UK*, 2018. https://www.thyssenkrupp-materials.co.uk/density-of-aluminium.html (accessed Jul. 20, 2025).

[36] “MIT and NASA engineers demonstrate a new kind of airplane wing,” *MIT News | Massachusetts Institute of Technology*, 2019. https://news.mit.edu/2019/engineers-demonstrate-lighter-flexible-airplane-wing-0401 (accessed Jul. 20, 2025).

[37] H. Maleki, L. Durães, C. A. García-González, P. del Gaudio, A. Portugal, and M. Mahmoudi, “Synthesis and biomedical applications of aerogels: Possibilities and challenges,” *Advances in Colloid and Interface Science*, vol. 236, pp. 1–27, Oct. 2016, doi: https://doi.org/10.1016/j.cis.2016.05.011.

[38] “NASA - NSSDCA - Experiment - Details,” *Nasa.gov*, 2024. https://nssdc.gsfc.nasa.gov/nmc/experiment/display.action?id=2023-098A-06 (accessed Jul. 21, 2025).

[39] “Curiosity Science Instruments - NASA Science,” *science.nasa.gov*. https://science.nasa.gov/mission/msl-curiosity/science-instruments/#h-chemistry-amp-camera-chemcam (accessed Jul. 21, 2025).
[40] C. Brown, H. Nagle, and D. Porterfield, “Title: Development of a Self-calibrating Dissolved Oxygen Microsensor Array for the Monitoring and Control of Plant Growth in a Space Environment MO).” Accessed: Jul. 22, 2025. [Online]. Available: https://ntrs.nasa.gov/api/citations/20040074348/downloads/20040074348.pdf
[41] “Tunable Laser Spectrometer on NASA’s Curiosity Mars Rover - NASA,” *nasa.gov*. https://www.nasa.gov/image-article/tunable-laser-spectrometer-nasas-curiosity-mars-rover/
[42] “Vaisala HUMICAP® Technology,” *Vaisala*. https://www.vaisala.com/en/vaisala-humicapr-technology (accessed Jul. 21, 2025).
[43] “Vaisala BAROCAP® Technology,” *Vaisala*, Aug. 23, 2024. https://www.vaisala.com/en/vaisala-barocapr-technology (accessed Jul. 22, 2025).
[44] NASA, “Perseverance science instruments - NASA Science,” *science.nasa.gov*, 2020. https://science.nasa.gov/mission/mars-2020-perseverance/science-instruments/ (accessed Jul. 20, 2025).
[45] J. N. Maki *et al.*, “The Mars 2020 Engineering Cameras and Microphone on the Perseverance Rover: A Next-Generation Imaging System for Mars Exploration,” *Space Science Reviews*, vol. 216, no. 8, Nov. 2020, doi: https://doi.org/10.1007/s11214-020-00765-9.
[46] in St, “Navigation Camera (Navcam),” *Wustl.edu*, 2022. https://an.rsl.wustl.edu/help/Content/About%20the%20mission/MER/Instruments/MER%20Navcam.htm (accessed Jul. 20, 2025).
[47] in St, “Navigation Camera (Navcam),” *Wustl.edu*, 2024. https://an.rsl.wustl.edu/help/Content/About%20the%20mission/MSL/Instruments/MSL%20Navcam.htm (accessed Jul. 20, 2025).
[48] “MARS INGENUITY,” *Onrender.com*, 2020. https://marsingenuity.onrender.com/ (accessed Jul. 21, 2025).
[49] X. Sun, “Space-Based Lidar Systems.” Accessed: Jul. 20, 2025. [Online]. Available: https://ntrs.nasa.gov/api/citations/20120012916/downloads/20120012916.pdf

[50] R. L. Kirk *et al.*, “Ultrahigh resolution topographic mapping of Mars with MRO HiRISE stereo images: Meter-scale slopes of candidate Phoenix landing sites,” vol. 113, Nov. 2008, doi: https://doi.org/10.1029/2007je003000.

[51] A. M. Barrett *et al.*, “NOAH-H, a deep-learning, terrain classification system for Mars: Results for the ExoMars Rover candidate landing sites,” *Icarus*, vol. 371, p. 114701, Jan. 2022, doi: https://doi.org/10.1016/j.icarus.2021.114701.

[52] C. Leo, “The Math Behind Convolutional Neural Networks | Towards Data Science,” *Towards Data Science*, Apr. 09, 2024. https://towardsdatascience.com/the-math-behind-convolutional-neural-networks-6aed775df076/ (accessed Jul. 21, 2025).

[53] GeeksforGeeks, “EpsilonGreedy Algorithm in Reinforcement Learning,” *GeeksforGeeks*, May 2020. https://www.geeksforgeeks.org/machine-learning/epsilon-greedy-algorithm-in-reinforcement-learning/ (accessed Jul. 20, 2025).

[54] G.-T. Tu and J.-G. Juang, “UAV Path Planning and Obstacle Avoidance Based on Reinforcement Learning in 3D Environments,” *Actuators*, vol. 12, no. 2, p. 57, Jan. 2023, doi: https://doi.org/10.3390/act12020057.

[55] P. Victor *et al.*, “Multi-Objective Reinforcement Learning-based Deep Neural Networks for Cognitive Space Communications.” Accessed: Jul. 21, 2025. [Online]. Available: https://ntrs.nasa.gov/api/citations/20170007958/downloads/20170007958.pdf

[56] F. Lv *et al.*, “Highly Accurate Visual Method of Mars Terrain Classification for Rovers Based on Novel Image Features,” *Entropy*, vol. 24, no. 9, p. 1304, Sep. 2022, doi: https://doi.org/10.3390/e24091304.

[57] J. B. Wright *et al.*, “Jezero crater, Mars: application of the deep learning NOAH-H terrain classification system,” *Journal of Maps*, vol. 18, no. 2, pp. 484–496, Aug. 2022, doi: https://doi.org/10.1080/17445647.2022.2095935.

[58] D. Helmick, A. Angelova, M. Livianu, and L. Matthies, “Terrain Adaptive Navigation for Mars Rovers.” Accessed: Jul. 23, 2025. [Online]. Available: https://www-robotics.jpl.nasa.gov/media/documents/HelmickAero07tanav.pdf

[59] “casper | AIG,” *Nasa.gov*, 2025. https://ai.jpl.nasa.gov/public/projects/casper/ (accessed Jul. 20, 2025).
[60] “Deep Q-Network (DQN) Agents - MATLAB & Simulink,” *www.mathworks.com*. https://www.mathworks.com/help/reinforcement-learning/ug/dqn-agents.html
[61] R. Tedrake, “Ch. 8 - Linear Quadratic Regulators,” underactuated.mit.edu, 2024. https://underactuated.mit.edu/lqr.html
[62] M. Kelly, “An Introduction to Trajectory Optimization: How to Do Your Own Direct Collocation,” *SIAM Review*, vol. 59, no. 4, pp. 849–904, Jan. 2017, doi: https://doi.org/10.1137/16m1062569.
[63] A. De Marchi and M. Gerdts, “Free finite horizon LQR: A bilevel perspective and its application to model predictive control,” *Automatica*, vol. 100, pp. 299–311, Feb. 2019, doi: https://doi.org/10.1016/j.automatica.2018.11.032.
[64] NASA, “Mars Reconnaissance Orbiter - NASA Science,” *science.nasa.gov*, Mar. 25, 2025. https://science.nasa.gov/mission/mars-reconnaissance-orbiter/ (accessed Jul. 20, 2025).
[65] “Moon to Mars Architecture.” Accessed: Jul. 20, 2025. [Online]. Available: https://www.nasa.gov/wp-content/uploads/2024/12/acr24-mars-edl-challenges.pdf?emrc=d99c3e
[66] Penn State Earth and Environmental Systems Institute, “Exploring Martian Atmosphere Weather with Spacecraft and Simulations,” *YouTube*, Mar. 15, 2023. https://www.youtube.com/watch?v=k-AntjMLxkA (accessed Jul. 21, 2025).
[67] W. Steigerwald, “First You See It, Then You Don’t: Scientists Closer to Explaining Mars Methane Mystery - NASA,” *NASA*, Jun. 29, 2021. https://www.nasa.gov/solar-system/first-you-see-it-then-you-dont-scientists-closer-to-explaining-mars-methane-mystery/ (accessed Jul. 20, 2025).
[68] “NASA Research Suggests Mars Once Had More Water Than Earth’s Arctic Ocean - NASA.” https://www.nasa.gov/news-release/nasa-research-suggests-mars-once-had-more-water-than-earths-arctic-ocean/ (accessed Jul. 20, 2025).